Cell

The Mitochondrial Phosphatase PGAM5 Functions at the Convergence Point of Multiple Necrotic Death Pathways

Zhigao Wang,[1] Hui Jiang,[1,2] She Chen,[2] Fenghe Du,[1] and Xiaodong Wang[1,2,*]
[1]Department of Biochemistry, University of Texas Southwestern Medical Center, 5323 Harry Hines Boulevard, Dallas, TX 75390, USA
[2]National Institute of Biological Sciences, 7 Science Park Road, Zhongguancun Life Science Park, Beijing 102206, China
*Correspondence: wangxiaodong@nibs.ac.cn
DOI 10.1016/j.cell.2011.11.030

SUMMARY

The programmed necrosis induced by TNF-α requires the activities of the receptor-interacting serine-threonine kinases RIP1 and RIP3 and their interaction with the mixed lineage kinase domain-like protein MLKL. We report the identification of RIP1- and RIP3-containing protein complexes that form specifically in response to necrosis induction. One component of these complexes is the mitochondrial protein phosphatase PGAM5, which presents as two splice variants, PGAM5L (long form) and PGAM5S (short form). Knockdown of either form attenuated necrosis induced by TNF-α as well as reactive oxygen species (ROS) and calcium ionophore, whereas knockdown of RIP3 and MLKL blocked only TNF-α-mediated necrosis. Upon necrosis induction, PGAM5S recruited the mitochondrial fission factor Drp1 and activated its GTPase activity by dephosphorylating the serine 637 site of Drp1. Drp1 activation caused mitochondrial fragmentation, an early and obligatory step for necrosis execution. These data defined PGAM5 as the convergent point for multiple necrosis pathways.

INTRODUCTION

Mitochondria are now recognized as cell death executors in addition to their more traditional roles in bioenergetics and metabolism. During apoptosis, cytochrome c, Smac/Diablo, Omi/HtrA2, EndoG, and AIF are released from the mitochondrial intermembrane space and elicit biochemical reactions leading to apoptosis (Wang and Youle, 2009). The permeability of the outer mitochondrial membrane to these apoptogenic factors is regulated by the Bcl-2 family of proteins. Antiapoptotic members of the Bcl-2 family, such as Bcl-2, Bcl-xL, and Mcl-1, bind and antagonize the homologous proapoptotic members of the family, including Bax and Bak, and the ''BH3-only'' members such as Bim, Bad, and Puma (which share homology with Bcl-2 only at the BH3 region) (Youle and Strasser, 2008). The current hypothesis proposes that the BH3-only proteins activate Bax and Bak, leading to Bax/Bak oligomerization into protein-permeable pores. However, direct evidence for these pores is still lacking.

Mitochondria are interconnecting cellular organelles that undergo dynamic changes in response to physiological and pathological changes. True to their bacterial origin, mitochondria undergo fission and fusion, which are processes controlled by a group of large GTPases. In mammalian cells, mitochondrial fusion is regulated by mitofusin-1 and -2 (MFN-1/2) and optic atrophy 1 (OPA1), whereas mitochondrial fission is controlled by a Dynamin-related protein 1, Drp1, and its mitochondrial anchors Fis1 and Mff (Otera and Mihara, 2011).

Once bound to mitochondria, Drp1 assembles into spirals at division sites around the outer mitochondrial membrane to drive the fission process (Smirnova et al., 2001). The activity of Drp1 is regulated by phosphorylation and dephosphorylation events. The phosphorylation by cyclic AMP-dependent kinase (PKA) at serine 637 site of human Drp-1 inhibits its GTPase activity and prevents mitochondrial fission (Chang and Blackstone, 2007; Cribbs and Strack, 2007).

Mitochondrial fragmentation has been observed during cell death (Frank et al., 2001). Emerging evidence points to an active role for mitochondrial fragmentation in apoptosis and necrosis. For example, loss of Drp1 function has been shown to slow down apoptosis and necrosis in *C. elegans* (Breckenridge et al., 2008; Jagasia et al., 2005). Inhibition of Drp1 and Fis1 activity delays cell death (Frank et al., 2001; Lee et al., 2004). Consistent with these results, boosting mitochondrial fusion by the overexpression of MFN1 and MFN2 inhibits apoptosis (Sugioka et al., 2004), and the downregulation of OPA1 induces the spontaneous apoptosis (Olichon et al., 2003).

The receptor-interacting kinase RIP3 is a critical signaling component for the cellular necrotic response to the TNF-α family of cytokines (Declercq et al., 2009). This form of necrotic cell death (also known as necroptosis) has been implicated in development, tissue damage during acute pancreatitis, retinal detachment, and antiviral immunity (Cho et al., 2009b; He et al., 2009; Kaiser et al., 2011; Oberst et al., 2011; Trichonas et al., 2010; Upton et al., 2010). The necrosis pathway downstream of RIP3 remains largely unknown, although ROS generation, calcium overload, and the opening of the mitochondrial permeability transition pore have been implicated (Vanlangenakker et al., 2008).

Taking advantage of a chemical compound, necrosulfonamide (Sun et al., 2011 [this issue of *Cell*]), which specifically inhibits TNF-α-mediated necrosis downstream of RIP3 activation and a cell line harboring a tagged version of functional RIP3 under the control of an inducible promoter, we identified multiprotein complexes that specifically formed after necrosis induction. Our results show that one of the components is the mitochondrial phosphoglycerate mutase/protein phosphatase PGAM5, which functions as a convergent point for multiple necrotic death pathways.

RESULTS

RIP3 Overexpression Augments TNF-α-Induced Necrosis

To characterize the role of RIP3 in necrosis, we generated a HeLa stable cell line that harbored a doxycycline (Dox)-inducible expression construct containing RIP3 fused to a 3xFlag tag and an HA tag at its N terminus. HeLa cells normally do not express RIP3. Addition of Dox to the culture media induced expression of RIP3 that was more than 20-fold higher than the basal level (leaky) expression of RIP3 transgene, which was about four times the level of endogenous RIP3 in human colon cancer HT-29 cells (Figure 1A). Before Dox addition, the basal expression of RIP3 transgene in HeLa cells made the cells behave similarly to HT-29 cells. The cells underwent necrosis when treated with the combination of TNF-α, the Smac mimetic and z-VAD-fmk, but remained alive when treated with TNF-α alone or TNF-α plus either Smac mimetic or z-VAD-fmk (Figure 1B; He et al., 2009). The necrosis was inhibited by an allosteric RIP1 kinase inhibitor necrostatin-1 and the mixed lineage kinase-like (MLKL) protein inhibitor necrosulfonamide (Degterev et al., 2008; Sun et al., 2011). With the addition of Dox, the cells underwent necrosis in response to TNF-α alone as well as to TNF-α plus either z-VAD-fmk and/or the Smac mimetic (Figure 1B). This observation is consistent with the previous findings that higher levels of RIP3 may cause cells to undergo necrosis in response to TNF-α alone, bypassing the requirement of z-VAD-fmk and Smac mimetic (He et al., 2009; Trichonas et al., 2010). Moreover, necrosis also proceeded faster upon Dox addition (Figure S1A available online).

Interestingly, the Dox-induced higher level of RIP3 expression abolished the ability of necrostatin-1 to efficiently block necrosis in these cells, although knockdown of its target RIP1 still attenuated necrosis (Figures 1B and S1B). It is likely that with higher level of RIP3, cells were able to overcome the allosteric inhibition of necrostatin-1 on RIP1. In contrast, necrosulfonamide still efficiently prevented necrosis under the same conditions (Figure 1B). Consistently, knockdown of MLKL in the Dox-treated HeLa cells also blocked necrosis (Figure S1B).

Necrosulfonamide Blocks Mitochondrial Fragmentation Associated with Necrosis

To monitor the morphological changes associated with TNF-α-induced necrosis in detail, we transiently expressed RFP-ANT1, a mitochondrial marker, and YFP-HMGB1, a nuclear marker, into the Dox-induced, RIP3-expressing HeLa cells. These cells were treated by the combination of TNF-α, Smac mimetic, and zVAD-fmk and analyzed with a spinning-disk confocal microscope. As shown in Figure 1C, the shape of nuclei and tubular mitochondria was normal before the treatment. After 120 min of treatment, the mitochondria became fragmented into small dots scattered throughout the cell, whereas the nuclear and cytoplasmic membranes were intact. At 360 min, the nuclear membrane broke down and the YFP signal dispersed into the cytosol, while the mitochondria formed clumps. By 580 min, the YFP signal eventually dissipated, indicating the breakdown of the plasma membrane.

Consistent with the observation that necrostatin-1 failed to block necrosis when RIP3 was overexpressed (Figure 1B), the addition of necrostatin-1 did not prevent the mitochondrial fragmentation and clustering as visualized by immunofluorescent staining of Tom20, another mitochondrial marker (Figure 1D). In contrast, in the presence of necrosulfonamide, the tubular mitochondrial morphology remained normal (Figure 1D). Consistently, knockdown of MLKL, the cellular target of necrosulfonamide, also prevented the mitochondrial morphological changes under necrosis-inducing conditions, whereas a control luciferase knockdown did not (Figure 1E).

RIP3 Forms a Protein Complex with PGAM5 upon Necrosis Induction

To search for RIP3 substrates that function in the necrosis pathway, we immunoprecipitated the Flag-tagged RIP3 from HeLa cells treated with the vehicle DMSO or necrosis-inducing agents (TNF-α/Smac mimetic/Z-VAD). We then performed an in vitro kinase assay by incubating γ-^{32}P ATP with the immune complex and analyzed the protein phosphorylation by SDS-PAGE and autoradiography. As shown in Figure 2A, a phosphate-labeled protein at the expected position of RIP3 was detected before necrosis induction, indicating that there is a basal level of RIP3 activity in living cells. After necrosis induction, two additional bands that migrated slightly above the 55 and 35 kDa markers also appeared (Figure 2A). The upper band was at the expected position of MLKL, a newly discovered substrate of RIP3 (Sun et al., 2011).

In order to get the molecular identity of the lower band, we first fractionated cell extracts by centrifugation. The RIP1/RIP3 complex was found to be more prominent in the heavy membrane fraction (pellet fraction after centrifugation at 15,000 × g) after necrosis induction, and the complex accumulated in the presence of necrosulfonamide (Figure 2B). We then immune-purified the RIP3-containing complex from the p15 fraction and resolved the accumulated RIP3 immunocomplex using a gradient SDS-PAGE gel. We subsequently identified all of the associated proteins by silver staining followed by mass spectrometry. As indicated in Figure 2C, the protein bands that specifically associated with RIP3 during necrosis were RIP1, RIP3, MLKL, and PGAM5, a mitochondrial phosphoglycerate mutase that uses alternative catalytic activity to function as a Ser/Thr phosphatase (Takeda et al., 2009). The major PGAM5 protein band ran at the same position as the ~35 kDa phospho-protein band identified in the in vitro kinase assay, suggesting that PGAM5 might be another substrate of RIP1/RIP3 necrosome. PGAM5 has been shown to localize to the outer membrane of mitochondria with its C terminus facing the cytoplasm (Lo and Hannink, 2008).

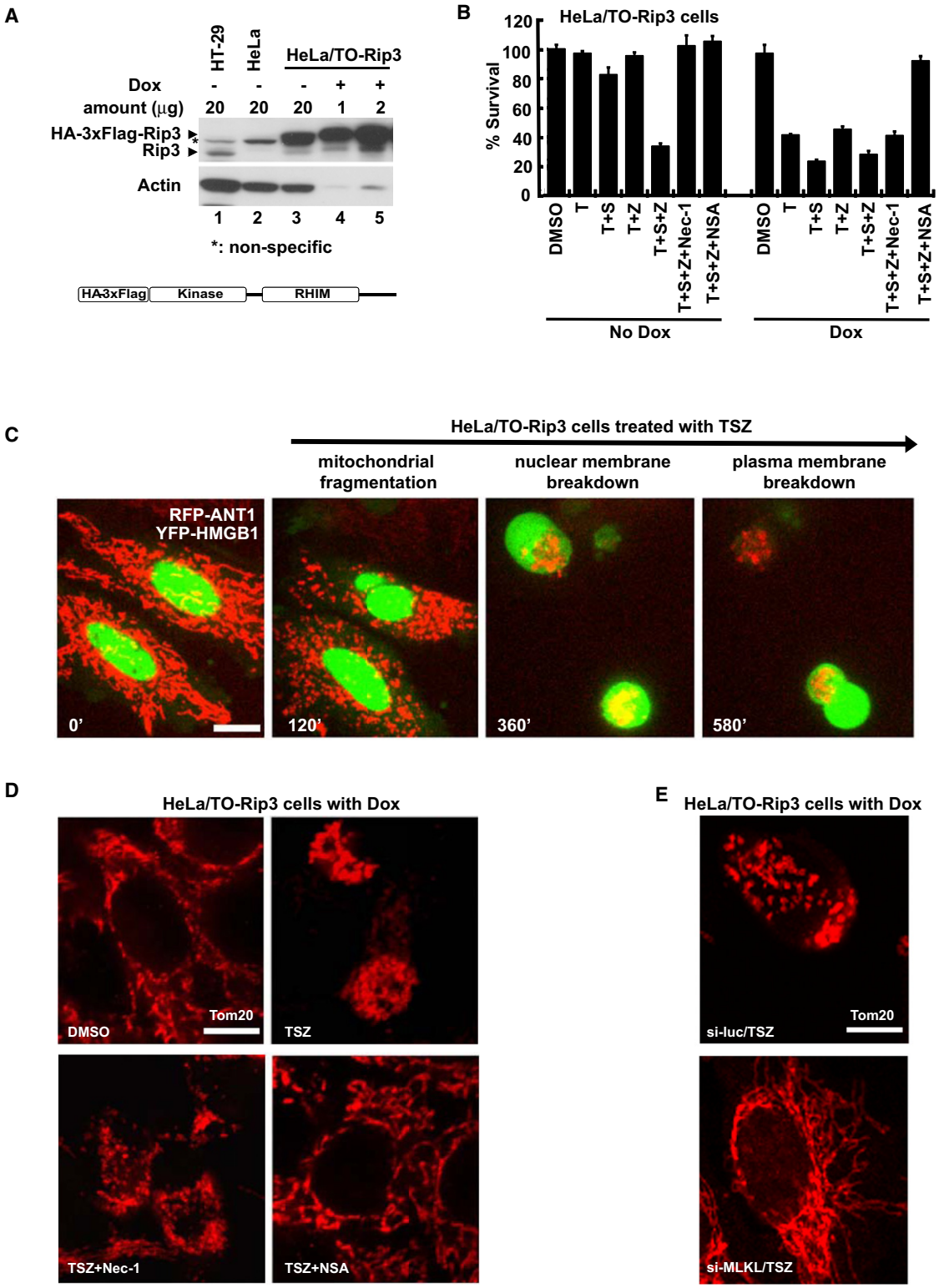

Figure 1. Necrostatin-1 and Necrosulfonamide Block TNF-α-Induced Necrosis at Different Steps

(A) Western blotting measurement of RIP3 levels before and after Dox-induced expression of stably transfected HA-3xFlag tagged RIP3 transgene in a HeLa cell line (HeLa/TO-Rip3).

(B) HeLa/TO-Rip3 cells with or without Dox induction were treated with the indicated necrosis-inducing agent(s) for 24 hr. Cell viability was determined using the CellTiter-Glo assay. TNF-α (20 ng/ml), 100 nM Smac mimetic, 20 μM Z-VAD, 10 μM necrostatin-1, and 2 μM necrosulfonamide were used. The same

To verify the specific association between RIP3 and PGAM5, we probed the RIP3 immunocomplex using an anti-PGAM5 antibody. Western blotting analysis of RIP1 and MLKL was also performed as controls. As shown in Figure 2D, similar to RIP1, the PGAM5 signal appeared in the complex only under necrosis-inducing conditions and increased in the presence of necrosulfonamide (lanes 1–3). In contrast, a kinase-dead form of RIP3 (K50A) failed to precipitate PGAM5 even though it still bound to RIP1 as previously observed (He et al., 2009). Similarly, the kinase-dead RIP3 also failed to interact with MLKL (Sun et al., 2011). The lower band of PGAM5 detected by western blotting might be a proteolytic or alternatively spliced form of PGAM5. The necrosis-specific association between PGAM5 and RIP1/RIP3 was further verified by a reciprocal pull-down experiment using an anti-PGAM5 antibody (Figure 2E).

To test if the association of PGAM5 with RIP1/RIP3 regulates the phosphatase activity of PGAM5, we immunoprecipitated RIP3 under normal or necrotic conditions and incubated the pellets with purified recombinant PGAM5 in an in vitro kinase and a phosphatase assay. As shown in Figure 2F, the recombinant PGAM5 was phosphorylated by the RIP3 complex under necrotic conditions. Interestingly, the phosphatase activity of recombinant PGAM5 showed significant increase after incubation with the RIP3 complex isolated under the necrotic conditions (Figure 2G).

Both Splice Variants of PGAM5 Are Required for Necrosis Execution

To verify the role of PGAM5 in necrosis execution, we performed siRNA knockdown of PGAM5 using two independent siRNA oligos targeting the coding region of PGAM5. Compared to a control luciferase siRNA oligo, knockdown of PGAM5 in the RIP3-expressing HeLa cells or HT-29 cells attenuated necrosis about 2-fold, and the efficiency of knockdown correlated with the degree of necrosis rescue (Figures 3A, 3B, and 3D). To further increase the knockdown efficiency, we also generated two HT-29 cell lines stably expressing each shRNA with the same sequences as the two siRNA oligos used for the transient knockdown. The PGAM5 was knocked down to a much lower level in these cells and nearly twice as many cells were rescued from necrosis compared to transient knockdown using siRNA oligos (Figures 3C and 3D). To rule out the off-target effects of these shRNAs, we attempted to rescue the PGAM5 knockdown by expressing an shRNA-resistant cDNA of PGAM5 (Figures 3C and 3D, last lane). To our surprise, the cells were still resistant to necrosis, although the shRNA-resistant cDNA of PGAM5 generated more PGAM5 protein than the endogenous PGAM5 (Figure 3D). The ectopically expressed PGAM5 should be functional since this form of PGAM5 in host cells accelerated necrosis and rendered them resistant to antinecrosis compounds (Figures S2A–S2C).

One possible explanation for such a result was that the shRNA-resistant cDNA used in the rescue experiment expressed only one of the two splice variants of PGAM5, whereas the shRNA targeted the common region of both isoforms. The inability of this isoform of PGAM5 to rescue shRNA knockdown suggested that both forms of PGAM5 participated in necrosis execution. To investigate such a possibility, we had to find a way to unambiguously distinguish these two spliced forms.

The alternative splicing made a truncation at amino acid residue 239 of the long form of PGAM5, PGAM5L, and an addition of 16 hydrophobic amino acid residues at the C terminus (Figure 3E; Lo and Hannink, 2006). These changes potentially rendered the short form of PGAM5, PGAM5S, more hydrophobic than PGAM5L. Therefore, we suspected that the extraction buffer we used for PGAM5L (containing 1% Triton X-100) did not extract PGAM5S. Since PGAM5L was often proteolyzed into several small fragments that overlapped in size with PGAM5S (Figure 2C), we had to individually engineer a Myc-tag into PGAM5S and PGAM5L to specifically study their distributions (Figure 3F). Indeed, we found that PGAM5S was not present in the Triton X-100 extractable fraction. We subsequently lysed the Triton X-100 insoluble pellet with a buffer containing 1% SDS and then diluted the 1% SDS-extracted soluble fraction into 0.1% SDS for the coimmunoprecipitation studies. As shown in Figure 3F, PGAM5S was only present in the 1% SDS-soluble fraction. The ability to specifically probe PGAM5L and PGAM5S allowed us to dissect the roles of these two splice forms in necrosis.

We designed siRNA oligos targeting the 3′-untranslated region of PGAM5 that specifically knocked down only one form of PGAM5. As shown in Figures 3E, 3G, and 3H, all of these siRNA oligos attenuated necrosis to a degree that correlated with the respective efficacy for PGAM5S or PGAM5L knockdown, confirming our hypothesis.

We then tried to rescue necrosis in shRNA-expressing HT-29 cells with double expression of shRNA-resistant PGAM5L and PGAM5S. The expression of both spliced forms of PGAM5 significantly rescued necrosis compared to either form alone (Figures 3I and S2).

Necrosulfonamide Blocks the Interaction between PGAM5S and RIP3

We next analyzed the specific interaction between RIP3 and PGAM5S. As shown in Figure 4A, RIP1, RIP3 and PGAM5L were coprecipitated with the anti-Myc (PGAM5S) antibody under necrotic conditions. Interestingly, necrosulfonamide completely

concentrations were used in all experiments unless otherwise stated. The CellTiter-Glo assay was used to determine the cell viability in all the subsequent experiment. Data are represented as the mean ± STDEV of duplicates. T, TNF-α; S, Smac mimetic; Z, Z-VAD; Nec-1, necrostatin-1; NSA, necrosulfonamide.

(C) Sequential morphological changes during necrosis. HeLa/TO-Rip3 cells were transfected with RFP-ANT1 and YFP-HMGB1 expression plasmids. At 24 hr, TSZ was added and live cell imaging was recorded. Bar equals 10 μm. For all the subsequent experiments, Dox was added to the HeLa/TO-Rip3 cells unless otherwise stated.

(D) HeLa/TO-Rip3 cells were treated as indicated for 6 hr, and immunostaining was preformed using an anti-Tom20 antibody. Representative fields were selected.

(E) HeLa/TO-Rip3 cells were transfected with an siRNA against luciferase (luc) or MLKL. After 48 hr, the cells were treated with TSZ for 6 hr, and immunostaining was preformed using an anti-Tom20 antibody.

See also Figure S1.

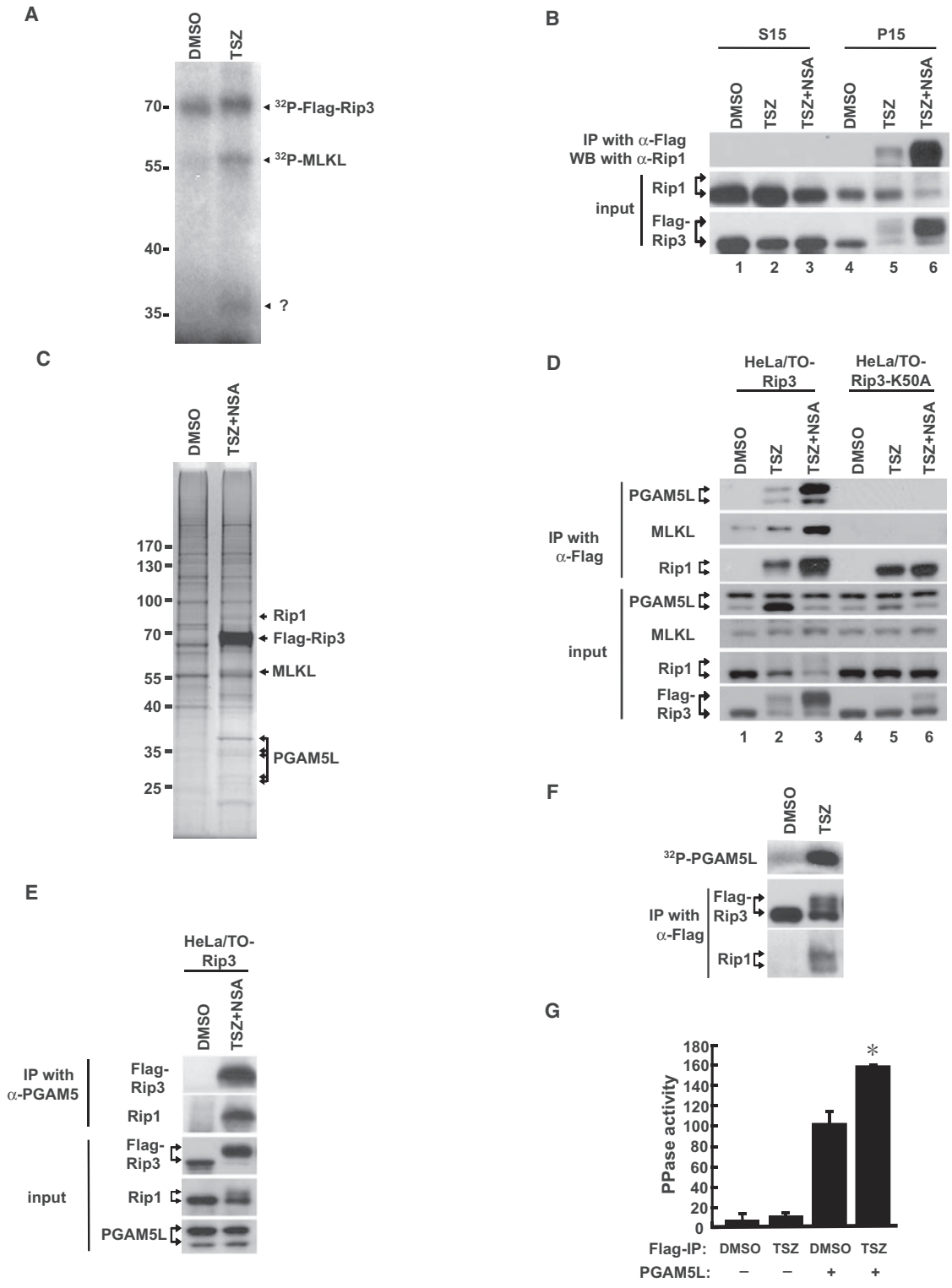

Figure 2. Mitochondrial Phosphatase PGAM5L Is a Kinase Substrate of RIP1/RIP3

(A) HeLa/TO-Rip3 cells were treated with DMSO or TSZ for 6 hr. Whole-cell extract was immunoprecipitated with anti-Flag agarose. The beads were then incubated with γ-^{32}P-ATP before eluted with SDS sample buffer and subjected to SDS-PAGE followed by autoradiography.

(B) S15 and P15 fractions were extracted from HeLa/TO-Rip3 cells and subjected to anti-Flag immunoprecipitation. The immunoprecipitant was eluted with 3× Flag peptide and analyzed by western blotting with indicated antibodies.

blocked the interaction between PGAM5S and RIP1/RIP3. Since necrosulfonamide did not affect PGAM5L interaction with RIP1/RIP3 (Figure 2D), we concluded that PGAM5S is the downstream effector of RIP1/RIP3/MLKL/PGAM5L complex and necrosulfonamide blocks necrosis by preventing PGAM5S from association with this complex.

The Phosphorylation of PGAM5L and PGAM5S during Necrosis Is Differentially Regulated by Necrosulfonamide

The association of both isoforms of PGAM5 with the RIP1/RIP3 kinase complex during necrosis suggested that PGAM5L/S might be the kinase substrates. To directly analyze the phosphorylation events of these proteins, we subjected the two protein-containing fractions to two-dimensional electrophoresis followed by western blot analysis. We probed the filter with anti-Flag (RIP3) antibody as a positive control because RIP3 is a known phosphoprotein and its upward shifts during necrosis could be readily shifted down by the phosphatase treatment (Figure S3). As shown in Figure 4B, an upward shift of molecular weight measured by SDS-PAGE and a leftward shift of negative charge measured by isoelectric focusing electrophoresis were observed for RIP3 after necrosis induction. Consistent with the previous notion that necrosulfonamide prevents necrosis downstream of RIP3, the presence of necrosulfonamide augmented these shifts of RIP3. These necrosis-associated changes were abolished by pretreatment of the extracts with λ-phosphatase, confirming that the changes were caused by phosphorylation of RIP3. When the same analysis was performed for PGAM5L and PGAM5S, both isoforms exhibited necrosis-induced phosphorylation similar to RIP3 (Figures 4C and 4D). Notably, the phosphorylation of PGAM5L was not affected by necrosulfonamide (Figure 4C, lower), whereas the phosphorylation of PGAM5S was totally abolished by the compound (Figure 4D, lower).

Because necrosulfonamide specifically targets MLKL (Sun et al., 2011), we analyzed the phosphorylation status of PGAM5S after MLKL knockdown. As shown in Figure 4E, MLKL knockdown also abolished PGAM5S phosphorylation similar to necrosulfonamide treatment. These results are consistent with a model that MLKL mediates the proper targeting of RIP1/RIP3 necrosome to its downstream effector PGAM5S.

Phosphorylation-Dependent Distribution of RIP1/RIP3 Complex in the SDS-Soluble Fraction

The specific distribution of PGAM5S in the SDS-soluble fraction indicated that that these locations might be the sites of mitochondrial fragmentation, which is an early event during necrosis (Figure 1C). We therefore analyzed the 1% SDS soluble fraction for the presence of RIP1/RIP3 and Drp1, which controls mitochondrial fission, a process that could lead to mitochondrial fragmentation. As shown in Figure 5A, RIP1 and RIP3 were shifted upward after necrosis induction, and the upward shifts accumulated in the presence of necrosulfonamide in the whole-cell extracts prepared by Triton X-100 extraction (lanes 1–3). The upward shifts were not observed in cells expressing the kinase-dead form of RIP3 (lanes 4–6). Interestingly, only the upward-shifted RIP1 and RIP3 ended up in the SDS-soluble fractions after necrosis induction (lanes 8 and 9). The proteolytic form of PGAM5L and Drp1 also appeared in the SDS-soluble fraction after necrosis induction. Upon necrosulfonamide treatment, PGAM5L and Drp1 were no longer detected in the SDS-soluble fraction, whereas RIP1 and RIP3 were not much affected. These results again confirmed that necrosulfonamide worked downstream of RIP1/RIP3 activation (lanes 8 and 9).

Drp1 Activation during Necrosis

The specific appearance of Drp1 in the 1% SDS-soluble fraction during necrosis suggested that Drp1 might function in the necrotic process. We further explored this possibility by monitoring its distribution during necrosis by immunostaining. As shown in Figure 5B, Drp1 was evenly distributed in the cytosol and partially colocalized with tubular mitochondria in DMSO-treated cells (top). After necrosis induction, mitochondria formed clumps around nucleus and Drp1 was greatly enriched on mitochondria (bottom).

Drp1 dephosphorylation at amino acid residue serine 637 indicates Drp1 activation (Chang and Blackstone, 2007; Cribbs and Strack, 2007). A phospho-specific antibody recognized the phosphorylation of this site (Figure 5C, lane 1). After necrosis induction, the phosphorylation signal was lost, whereas necrosulfonamide blocked the dephosphorylation of S637 during necrosis (lanes 2 and 3). The total amount of Drp1 did not change significantly during necrosis (Figure 5C). In addition to S637 dephosphorylation, activated Drp1 formed dimers through disulfide linkage of monomers (Cho et al., 2009a). Necrosis induction also increased dimer formation of Drp1, which was attenuated by necrosulfonamide (Figure 5D).

To directly demonstrate Drp1 activation during necrosis, we immunopurified Drp1 from control and necrotic cells and measured its GTPase activity. As shown in Figure 5E, the GTPase activity of Drp1 was significantly increased during necrosis, which was inhibited by necrosulfonamide.

(C) HeLa/TO-RIP3 cells were treated as indicated for 6 hr. The P15 fraction was used for anti-Flag and anti-HA tandem pull-downs. The final eluates were separated on a 4%–12% gradient gel and detected by silver staining. The indicated protein bands were identified by mass spectrometry.

(D) HeLa/TO-Rip3 or HeLa/TO-Rip3-K50A (a similarly generated cell line expressing a kinase-dead form K50A of RIP3) cells were treated as indicated for 6 hr and the P15 fraction was used for anti-Flag immunoprecipitation. The immunoprecipitant was eluted with 3 × Flag peptide and analyzed by western blotting using the indicated antibodies.

(E) HeLa/TO-Rip3 cells were treated as indicated for 6 hr. The P15 fraction was used for immunoprecipitation with an anti-PGAM5 antibody. The immune complexes were analyzed by western blotting using the indicated antibodies.

(F) HeLa/TO-Rip3 cells were treated as indicated for 6 hr. Whole-cell extracts were used for anti-Flag immunoprecipitation. The immune complexes were either analyzed by western blotting for RIP3 (Flag) or RIP1, or incubated with γ-^{32}P-ATP and 100 ng of recombinant His-PGAM5L (88–289). The phosphorylated PGAM5L was analyzed by SDS-PAGE followed by autoradiography (top).

(G) An in vitro kinase assay for PGAM5L was performed as in (F) with cold ATP. The phosphatase activity was then measured as described in Experimental Procedures. *$p < 0.05$.

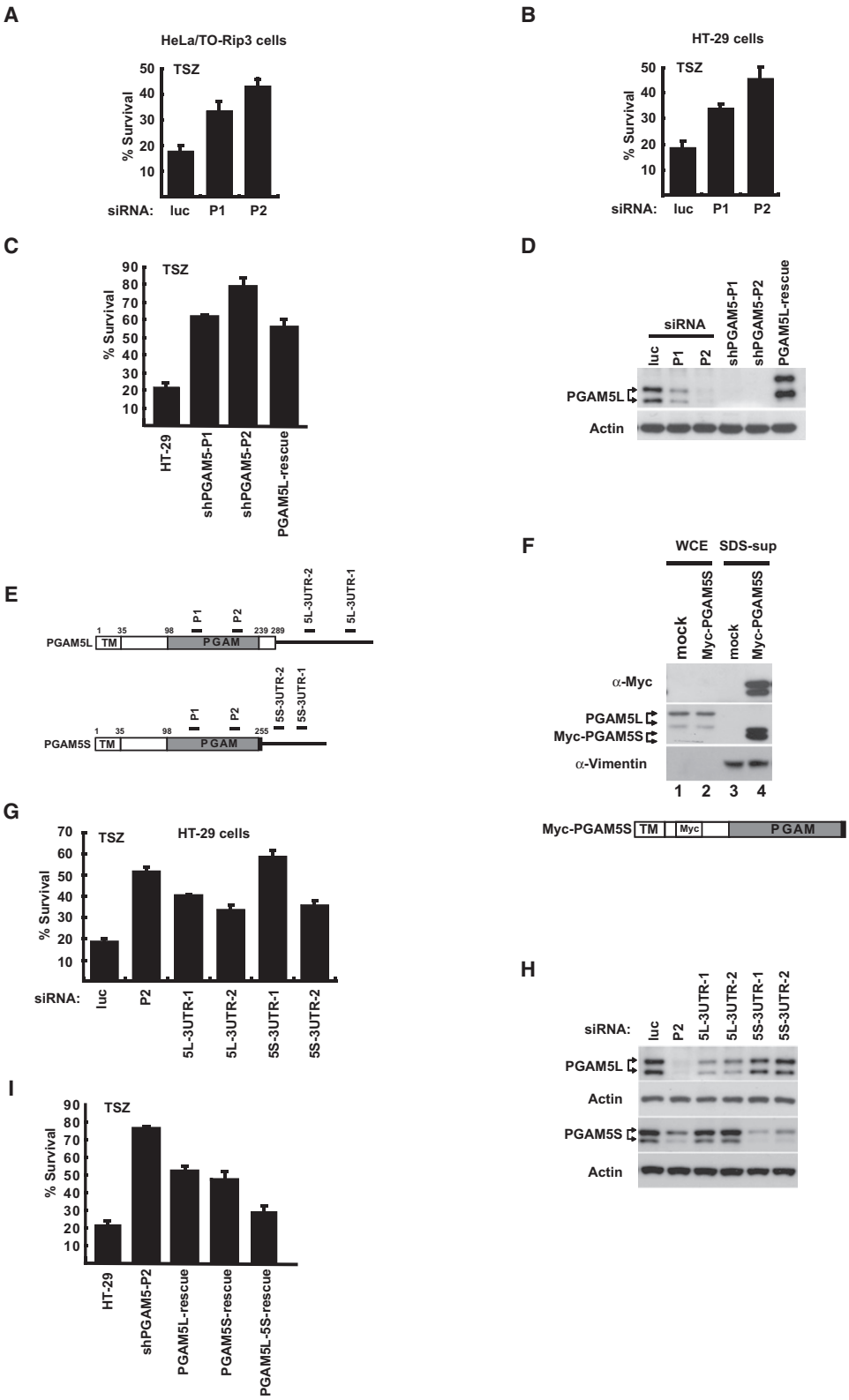

Figure 3. Both PGAM5L and PGAM5S Are Required for TNF-α-Induced Necrosis

(A and B) HeLa/TO-Rip3 cells (A) or HT-29 cells (B) were transfected with siRNAs against luciferase (luc) or PGAM5 (P1 and P2) for three rounds. Cell viability was determined after 24 hr of TSZ treatment.

PGAM5S Recruits and Activates Drp1 on Mitochondria

To test whether the activation of Drp1 during necrosis requires PGAM5, we first tested the possibility that PGAM5S directly recruited Drp1 to mitochondria. To this end, we ectopically expressed Myc-tagged PGAM5L and PGAM5S separately in the RIP3-expressing HeLa cells and immunoprecipitated them with an anti-Myc antibody. The immune complexes were subsequently probed with antibodies against Myc and Drp1. As shown in Figure 5F, Drp1 was specifically coprecipitated with PGAM5S but not PGAM5L although similar amount of each was precipitated by the anti-Myc antibody.

To directly demonstrate that PGAM5 dephosphorylated Drp1 and activated its GTPase activity, we incubated purified wild-type recombinant PGAM5L or a phosphatase dead (H105A) form with the immunopurified Drp1. PGAM5L was used as a surrogate for PGAM5S because recombinant PGAM5S was not soluble in the assay buffer and the enzymatic portions of these two proteins are identical. As shown in Figures 5G and 5H, respectively, the wild-type PGAM5L dephosphorylated Drp1 at serine 637 and dramatically increased its GTPase activity, whereas the phosphatase-dead form of PGAM5L did not cause these changes.

Knockdown of PGAM5S Attenuates Drp1 Activation

To further characterize the specific role of PGAM5S in activating Drp1, we measured Drp1 distribution and activation markers in cells stably expressing an shRNA targeting the unique 3′-untranslated region of PGAM5S (Figure 3E). Knockdown of PGAM5S prevented necrosis and necrosis-associated mitochondrial fragmentation and aggregation (Figures 6A and 6B). The preventative effect of PGAM5S knockdown was not caused by an off-target effect of the shRNA because expressing the shRNA-resistant wild-type PGAM5S but not the phosphatase-dead (H105A) form rescued necrosis in these cells (Figures 6A and S4). In these PGAM5S knockdown cells, appearance of proteolytic form of PGAM5L and Drp1 in the 1% SDS-soluble fraction during necrosis was also eliminated (Figure 6C, compare lanes 8 and 11). Consistently, Drp1 dephosphorylation at S637 and Drp1 dimerization, the two markers for its activation, were significantly attenuated in these cells (Figures 6D and 6E).

Drp1 Is Required for Necrosis Induction

The necrosis-dependent association of Drp1 with PGAM5S and Drp1 activation suggested that Drp1 might be required for necrosis execution. To further demonstrate this point, we treated HT-29 cells and the RIP3-expressing HeLa cells with a Drp1 inhibitor mdivi-1 (Cassidy-Stone et al., 2008). Necrosis was attenuated in both cell lines with increasing concentrations of mdivi-1 (Figure 6F). Additionally, knockdown Drp1 in both cell lines blocked necrosis (Figure 6G).

These data suggested that PGAM5S is a central necrosis mediator. It connects the upstream necrosome with Drp1 during necrosis (Figure 6H and see more in the Discussion section).

PGAM5 Functions in Multiple Necrotic Pathways

The cell lines with stable knockdown of PGAM5L and/or PGAM5S provided us with an opportunity to study their roles in cell death induced by other agents. For example, t-butyl hydroxide (TBH), a ROS generator, also induced mitochondrial fragmentation and clustering around nuclei at a concentration of 100 μM (Figure 7A). The pan-caspase inhibitor zVAD-fmk augmented cell death, indicating that cell death was mediated by necrosis not apoptosis (Figure 7B). As expected, a ROS scavenger, N-acetyl-L-cysteine (NAC), attenuated cell death to some extent (Figure 7B). Interestingly, the majority of cells expressing the shRNA against PGAM5 (both forms) survived 100 μM TBH treatment (Figure 7C). Approximately 30% of these cells also survived 5 mM hydrogen peroxide treatment, a harsh condition that wiped out all the parental HT-29 cells (Figure 7D). In contrast, RIP3 knockdown did not prevent TBH- or H_2O_2-induced cell death.

Another common inducer of necrotic death is a calcium ionophore that produces transient calcium flashes in cells. Treatment of HT-29 cells with the calcium ionophore A23187 and the caspase inhibitor z-VAD-fmk caused more than 80% of treated cells to die (Figure 7E). Knockdown of RIP3 did not affect this form of cell death. However, 50%–60% of HT-29 cells that stably expressed shRNA against PGAM5 survived the treatment of A23187 and z-VAD-fmk.

These data suggested that PGAM5 might be the converging point of multiple necrosis pathways. The extrinsic signal such as TNF-α activates necrosis by engaging the RIP1/RIP3/MLKL necrosome pathway leading to the activation of PGAM5 and Drp1. The intrinsic necrosis-inducing signals such as TBH and A23187 might be able to activate PGAM5 and Drp1 independent of RIP1/RIP3/MLKL.

To further test this hypothesis, we knocked down RIP1, RIP3, MLKL, Drp1, PGAM5L, and PGAM5S before treating

(C) HT-29 stable cell lines expressing P1 or P2 shRNA were generated as described in Experimental Procedures. Myc-PGAM5L with silent mutation of the shRNA targeting site was stably expressed in the shPGAM5-P2 cells to generate the PGAM5L-rescue cell line. Cell viability was determined after 24 hr of TSZ treatment.
(D) Western blotting was used to measure the knockdown efficiency in (B) and (C).
(E) Schematic representation of the siRNAs used for PGAM5L and PGAM5S.
(F) PGAM5S is localized in an SDS-soluble domain. HeLa cells were transfected with a plasmid expressing Myc-PGAM5S. After isolating whole-cell extracts (WCEs), the pellet was further extracted with 1% SDS. Western blotting was performed with anti-Myc, anti-PGAM5, and antivimentin antibodies.
(G) HT-29 cells were transfected with three rounds of siRNA oligos targeting regions specific for either PGAM5L or PGAM5S as indicated, and cell viability was determined after 24 hr of TSZ treatment.
(H) Comparing the knockdown efficiency of isoform specific siRNA oligos used in (G). For PGAM5L, HeLa cells were transfected with the siRNAs for two rounds and WCE was used for western blotting. For PGAM5S, an expression plasmid including the coding region and 3′-untranslated region of PGAM5S was cotransfected with the siRNAs into HeLa cells. After 72 hr, the WCE was discarded, and the cell pellet was directly boiled in 1 × SDS loading buffer. Western blotting was performed with anti-PGAM5 and anti-β-actin antibodies.
(I) Myc-PGAM5S construct was stably expressed in the shPGAM5-P2 cells to generate the PGAM5S-rescue cell line. The same construct was stably expressed in the PGAM5L-rescue cells to generate PGAM5L-5S double rescue cell line. Cell viability was determined after 24 hr of TSZ treatment. Data are represented as the mean ± STDEV of duplicates.
See also Figure S2.

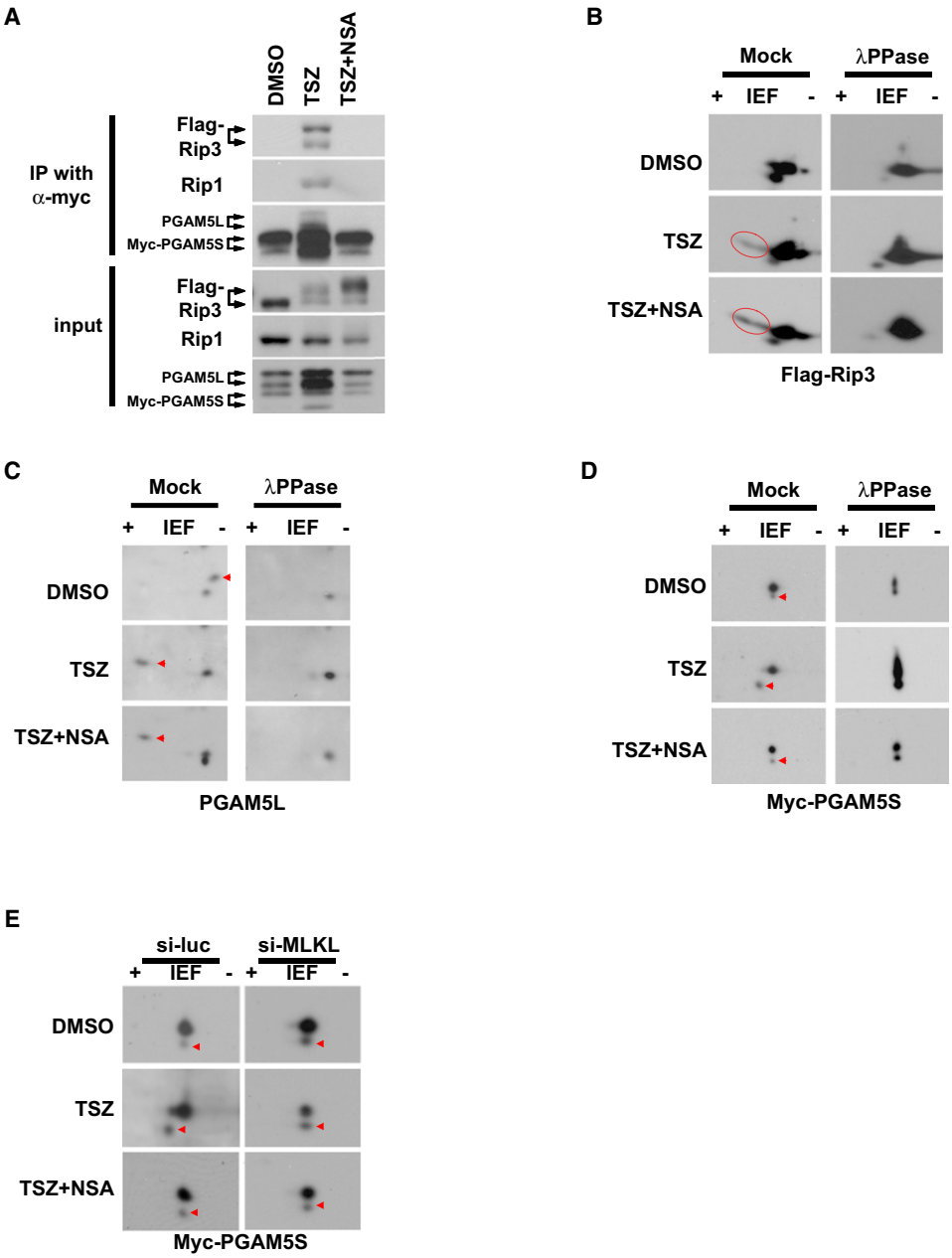

Figure 4. PGAM5L and PGAM5S Are Differentially Regulated during TNF-α-Induced Necrosis

(A) HeLa/TO-Rip3 cells were transfected with a plasmid expressing Myc-PGAM5S. The pellet after WCE was further extracted with 1% SDS. The SDS-extract was diluted ten times with lysis buffer and then mixed with WCE for anti-Myc immunoprecipitation. The immunoprecipitant was eluted with Myc peptide. Equal volume of WCE and SDS-extract were mixed as input. Western blotting was performed with anti-Flag, anti-RIP1, and anti-PGAM5 antibodies.

(B and C) HeLa/TO-Rip3 cells were treated as indicated for 6 hr. The WCE lysates before and after λPPase treatment were subjected to 2D electrophoresis. Western blotting was performed with anti-Flag antibody (B) or anti-PGAM5 antibody (C).

(D) HeLa/TO-Rip3 cells were transfected with a plasmid expressing Myc-PGAM5S and treated as indicated for 6 hr. PGAM5S was extracted as in Figure 3F and subjected to 2D electrophoresis. Western blotting was performed using anti-Myc antibody.

(E) HeLa/TO-Rip3 cells were transfected with a plasmid expressing Myc-PGAM5S and an siRNA against MLKL. After 48 hr, 2D electrophoresis was performed as described in (D).

See also Figure S3.

the cells with these intrinsic necrosis stimuli. As shown in Figures 7F–7H, knockdown of Drp1, PGAM5L, and PGAM5S, either individually or together, attenuated cell death induced by TBH, H_2O_2, and A23187. In contrast, knockdown of RIP1, RIP3, and MLKL did not affect cell death induced by these agents.

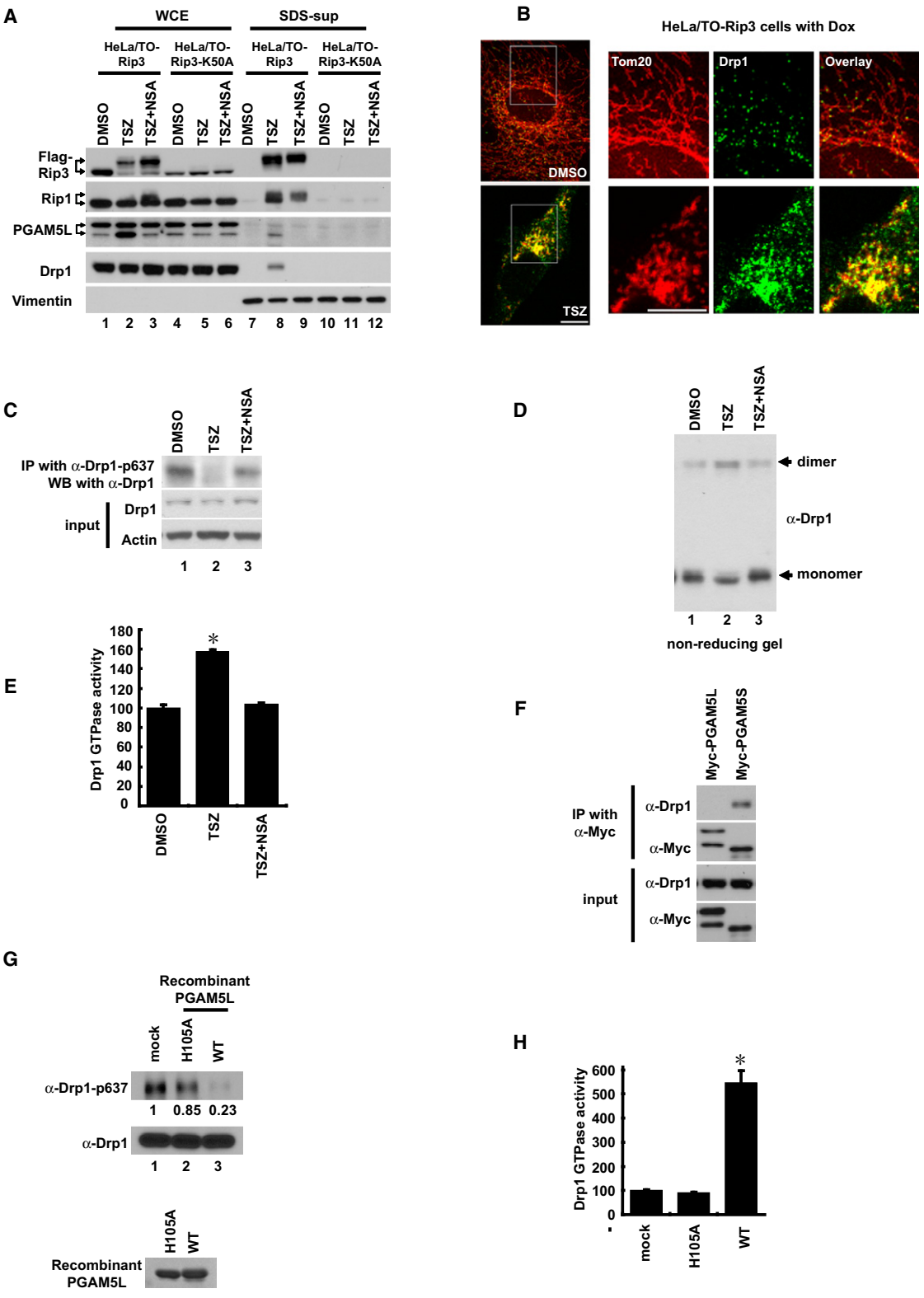

Figure 5. Drp1 Is Activated by PGAM5 upon Necrosis Induction

(A) Cells were treated as indicated for 6 hr. WCE and SDS-sup were isolated as described in Figure 3F and subjected to western blotting analysis with indicated antibodies.

Similar results were obtained in mouse embryonic fibroblast cells, suggesting that the same mechanism applies to other mammalian systems (Figure S5).

Staurosporine-induced apoptotic death was not affected by PGAM5 knockdown, indicating that PGAM5 might be specifically required for necrotic death (Figure S6).

DISCUSSION

PGAM5 at the Convergent Point of Extrinsic and Intrinsic Pathways of Necrosis

Our experimental data indicate that the two splice variants of the mitochondrial protein phosphatase PGAM5 are at the convergent point of multiple necrosis pathways. Similar to apoptosis that is initiated extrinsically by ligands for death receptors and intrinsically by BH3-only proteins, necrosis can also be triggered by both extrinsic and intrinsic signals. The extrinsic necrosis pathway relies on necrosome components consisting of the kinases RIP1, RIP3, and mixed lineage kinase domain-like protein MLKL (He et al., 2009; Holler et al., 2000; Sun et al., 2011). Downstream of the necrosome are two isoforms of PGAM5, which specifically associate with the necrosome after necrosis induction, resulting in PGAM5 phosphorylation and activation.

In contrast to extrinsic signals, the kinases RIP1 and RIP3, as well as MLKL, are not involved in the forms of necrosis that are induced by ROS generators or calcium ionophore (Figure 7). These signaling proteins are specific for the extrinsic necrosis (necrosome) pathway. However, both isoforms of PGAM5 function in the intrinsic necrosis pathway, based on the evidence that PGAM5 knockdown attenuates ROS- and calcium ionophore-induced necrotic death.

Activation Model for PGAM5L and PGAM5S during Necrosis

We propose that PGAM5L and PGAM5S are activated in a three-stage model in the extrinsic necrosis pathway (Figure 6H). The first stage is the formation of necrosome that is initiated by the activation of TNFR and the formation of the RIP1-containing signaling complex (complex I), which primarily functions to activate NF-κB (Micheau and Tschopp, 2003). The conversion of the membrane-associated complex I to the cytoplasmic complex II is mediated by the following: deubiquitylation of RIP1 by the deubiquitin enzyme CYLD; cIAPI/II degradation, which is triggered by Smac or Smac mimetics (Wang et al., 2008); and the binding of RIP3 and MLKL to the RIP1-containing complex (He et al., 2009; Sun et al., 2011). The successful formation of this complex requires the inhibition of caspase-8, which is also recruited to the RIP1-containing complex for activation (Wang et al., 2008).

The second stage of this necrosis pathway is the binding of PGAM5L to the necrosome. Notably, the binding of PGAM5L is not affected by the presence of the necrosis inhibitor necrosulfonamide. Necrosulfonamide arrests the necrosis-inducing protein signaling complex at this step, allowing the stable association of PGAM5L with the necrosome, which manifest as discrete cytosolic punctae (Sun et al., 2011). At this stage, the early RIP1 associated proteins including TRADD, FADD, Caspase-8, and Flip are no longer stoichiometric components of the complex (Figure 2C). The complex might loosely associates with mitochondria at this point, although the stoichiometry may not allow complete colocalization.

The third step is the association of this complex with PGAM5S. The compound necrosulfonamide blocks the binding of PGAM5S to the RIP1/RIP3/MLKL/PGAM5L complex. Consistently, the necrosis-associated phosphorylation of PGAM5S does not occur in the presence of necrosulfonamide, whereas phosphorylation of PGAM5L is not affected (Figure 4). PGAM5S is normally located in a more hydrophobic environment on mitochondria and becomes associated with the upstream necrosis-inducing complex probably through interactions with RIP3 and/or PGAM5L, resulting in the activation of PGAM5S by phosphorylation. Along this process, PGAM5L may also become proteolyzed before binding to PGAM5S.

The binding of the necrosome to PGAM5S marks its translocation to a more hydrophobic environment or the formation of larger aggregates that are soluble in 1% SDS but not 1% Triton X-100. The candidates for these hydrophobic locations are the constriction sites for mitochondrial fission where Drp1 forms 27 nm tubules (Yoon et al., 2001).

Drp1 Is Part of Necrosis Execution

Consistent with our model, Drp1 was activated during TNF-induced necrosis, which was measured by its dephosphorylation

(B) HeLa/TO-Rip3 cells were treated with DMSO (top) or TSZ (bottom) for 6 hr. Immunostaining was performed with rabbit anti-Tom20 (Red) and mouse anti-Drp1 (Green) antibodies. Bar equals 10 μm.

(C) HeLa/TO-Rip3 cells were treated as indicated for 6 hr. Whole-cell extracts were used for immunoprecipitation with anti-Drp1-p637 antibody. The immune complexes were analyzed by western blotting with a mouse anti-Drp1 antibody.

(D) HeLa/TO-Rip3 cells were treated as indicated for 6 hr. Whole-cell extracts were subjected to a nonreducing SDS-PAGE followed by western blotting analysis with an anti-Drp1 antibody.

(E) HeLa/TO-Rip3 cells were treated as indicated for 6 hr. GTPase activity of the immunopurified Drp1 was measured as described in Experimental Procedures. *$p < 0.05$.

(F) HeLa/TO-Rip3 cells were transfected with a plasmid expressing Myc-PGAM5L or Myc-PGAM5S. For Myc-PGAM5L expressing cells, WCE was directly used for anti-Myc immunoprecipitation. For Myc-PGAM5S expressing cells, the pellet after WCE was further extracted with 1% SDS. The SDS-extract was diluted ten times with lysis buffer and then mixed with WCE for immunoprecipitation with anti-Myc agarose. The immune complexes were analyzed by western blotting using antibodies against Myc (for PGAM5) and Drp1.

(G) Immunoprecipitated Drp1 was incubated with 3 μg of recombinant His-PGAM5L (22–289) or H105A mutant at 30°C for 6 hr. The beads were then subjected to western blotting with anti-Drp1 and anti-Drp1-p637 antibodies. The intensity of the western blotting signal was quantified with a Kodak Image Station 4000R Pro machine. The relative intensity was labeled under each lane.

(H) Drp1 immunoprecipitation and incubation with recombinant PGAM5L were performed similarly as described in (G). The beads were then subjected to the GTPase activity assay. *$p < 0.05$.

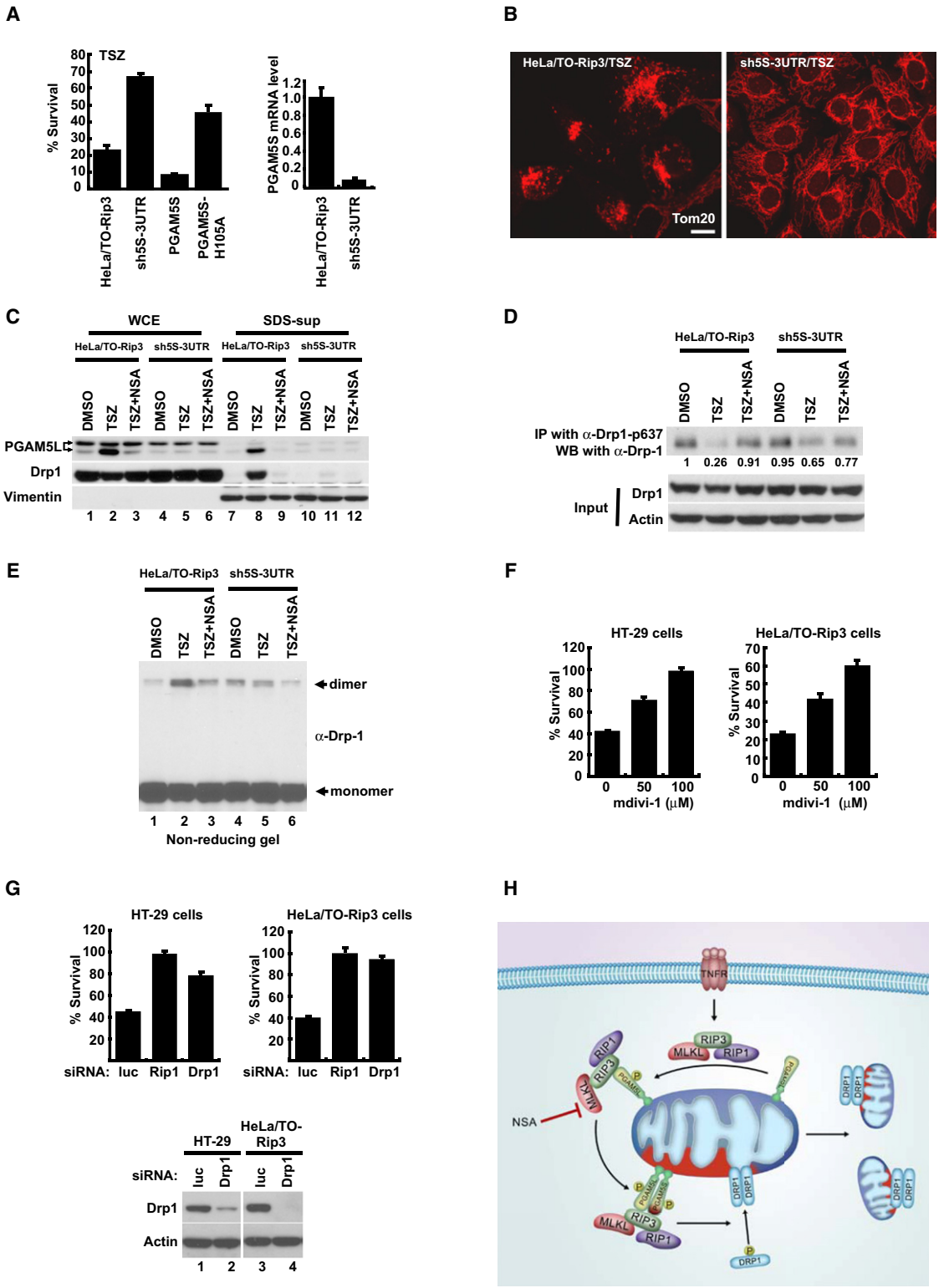

Figure 6. Drp1 Is Required for TNF-α-Induced Necrosis

(A) A stable cell line expressing shRNA against PGAM5S was generated in the HeLa/TO-Rip3 cells. Stable rescue cell lines expressing Myc-PGAM5S or Myc-PGAM5S-H105A were established in the sh5S-3UTR cells. Cell viability was determined after 24 hr of TSZ treatment (left). Knockdown efficiency was assayed using quantitative RT-PCR (right).

(B) The cells were treated with TSZ for 6 hr and immunostaining was performed with anti-Tom20 antibody. Bar equals 10 μm.

at serine 637, dimer formation, and elevated GTPase activity. All of these biochemical features are blocked by the necrosis inhibitor necrosulfonamide, indicating that the activation of Drp1 is a downstream event. These necrosis-associated changes are likely to be directly caused by PGAM5S. Because PGAM5S is hydrophobic and not compatible with biochemical assays in vitro, it is difficult to experimentally test the ability of PGAM5S to directly dephosphorylate and activate Drp1. Nevertheless, purified recombinant PGAM5L dephosphorylated and activated Drp1 (Figure 5). Because both isoforms of PGAM5 may eventually function in one large complex at the constriction sites of mitochondrial fission, Drp1 may be activated in situ at these sites.

Drp1-mediated mitochondrial fragmentation seems to be a common required step for apoptosis and necrosis. For apoptosis, mitochondrial fragmentation may be involved in mitochondrial outer membrane permeabilization, leading to cytochrome c release and caspase activation. During necrosis, mitochondria fragment and subsequently cluster around nuclei before nuclear and cytoplasmic membrane breakdown, the terminal stage of necrosis (Figure 1C). Yet, cytochrome c is not released during TNF-induced necrosis (Temkin et al., 2006), suggesting that the downstream event following mitochondrial fragmentation could be different between apoptosis and necrosis.

Another interesting feature of PGAM5L is that it is a substrate for Keap-1, a thiol-reactive sensor for ROS, and a substrate adaptor protein for a Cul3-dependent ubiquitin ligase complex (Lo and Hannink, 2008). It is conceivable that the PGAM5L/Keap-1 complex might be an effector for ROS-induced necrosis. However, the detailed mechanism requires further study. The link between calcium ionophore and PGAM5 is also unclear, but the molecular reagents described here should allow us to explore this topic in the future. The importance of these studies is highlighted by the finding that the loss of PGAM5 homolog in *Drosophila* suppresses the effects of inactivation of early Parkinson-responsible gene product PINK1, including mitochondrial degeneration, motor defects, and the shortened life span (Imai et al., 2010).

How mitochondrial fragmentation mediated by Drp1 causes necrosis is still not clear. Mitochondrial fragmentation may reduce energy production, increase ROS generation, or activate yet to be defined downstream necrosis execution steps. Therefore, the challenge remains to elucidate the other biochemical steps that are required for necrosis execution, either downstream of PGAM5 and Drp1 or in parallel.

EXPERIMENTAL PROCEDURES

Reagents

TNF-α and the Smac mimetic were prepared as previously described (He et al., 2009). Z-VAD-fmk was from Bachem, and Necrostatin-1 from Alexis Biochemicals. λ-Phosphatase was from NEB. Mdivi-1, A23187, Anti-Flag-M2-agarose (A1205), anti-HA-agarose (A2095), and anti-c-Myc-agarose (A7470) were from Sigma. The following antibodies were used: anti-Flag (Sigma, A8592), anti-c-Myc (Santa Cruz, sc-47694), anti-HA (Santa Cruz, sc-805), anti-RIP1 (BD Biosciences, 610458), anti-Tom20 (Santa Cruz, sc-11415), anti-MLKL (Sigma, M6697), anti-Drp1 (Santa Cruz, sc-101270 and sc-32989; Abcam, ab56788), and anti-phospho-Drp1 (ser637) (Cell Signaling, 4867). Anti-PGAM5 polyclonal antibody was generated against a fragment encoding the amino acid residues 89–289 of PGAM5L.

siRNA Transfection and CellTiter-Glo Assay

To improve the knockdown efficiency, three rounds of siRNA transfection were performed for mitochondrial genes. On day 0, cells were split into a 6-well plate at a density of 40,000 cells/well and transfected with 200 pmol siRNA in each well. On day 2, another 200 pmol siRNA was transfected. On day 4, the cells were split into a 96-well plate at a density of 2,000 cells/well and transfected with 10 pmol siRNA in each well. On day 6, the cells were treated as indicated. On day 7, the CellTiter-Glo assay was performed according to the manufacturer's instructions (Promega, G7570). For other treatments, 4,000 cells were plated into each well of a 96-well plate. Luminescence was measured using a "Synergy HT" machine from Biotek. Vehicle (DMSO) treatment was assigned as 100 percent, and the experimental treatment was divided by the vehicle treatment to calculate the percentage of cell survival. For all of the CellTiter-Glo assays, the mean ± STDEV of duplicates were presented.

Stable Cell Lines

Stable cell lines expressing the Tet repressor (TetR) were selected with 10 μg/ml Blasticidin after being transfected with the pcDNA6/TR plasmid from Invitrogen. HeLa-TetR cells were transfected with a pCDNA3 plasmid encoding HA-3xFlag-Rip3 and selected with 1 mg/ml G418 to establish the HeLa/TO-Rip3 cell line. The same strategy was used to establish the HeLa/TO-Rip3-K50A cell line. Stable lines with inducible shRNA expression were established as previously described (Zhong et al., 2005). Briefly, multiple copies of shRNA under the control of the H1 promoter were cloned into the pSuperior.puro vector (Oligoengine). The shRNA expressing plasmids were then transfected into the TetR cells and selected with 0.5 μg/ml puromycin. Rescue cell lines were established in the shRNA expressing cells using scramble expression constructs that were resistant to the shRNAs and contained hygromycin-resistant cassettes.

Immunoprecipitation

Cell extract was mixed with anti-Flag, anti-Myc, or anti-HA agarose beads in a ratio of 1 mg of extract per 30 μl of agarose at 4°C overnight. The beads were then pelleted at 2,500 × g for 3 min and washed with lysis buffer five times. The beads were subjected to elution with 5 vol of 0.5 mg/ml peptide for 4 hr or directly boiled in 1 × SDS loading buffer.

(C) The cells were treated as indicated for 6 hr. WCE and SDS-sup were harvested as in Figure 3F and analyzed by western blotting using the indicated antibodies.
(D) The cells were treated as indicated for 6 hr. Whole-cell extract was subjected to immunoprecipitation with anti-Drp1-p637 antibody. Western blotting was performed with an anti-Drp1 antibody. The relative intensity was labeled under each lane.
(E) The cells were treated as indicated for 6 hr. Whole-cell lysates were subjected to a nonreducing SDS-PAGE gel separation followed by western blotting analysis using an antibody against Drp1.
(F) The indicated cells were pretreated with different concentrations of mdivi-1 for 1 hr. TSZ were added for additional 14 hr and cell viability was measured.
(G) The indicated cells were transfected with three rounds of siRNAs against Luc, or RIP1, or Drp1. Cell viability was measured after 14 hr of TSZ treatment. Data are represented as the mean ± STDEV of duplicates. Western blotting was performed to assay the knockdown efficiency.
(H) Working model. Red region represents the mitochondrial SDS-soluble domain.
See the text for details. Supported by Figure S4.

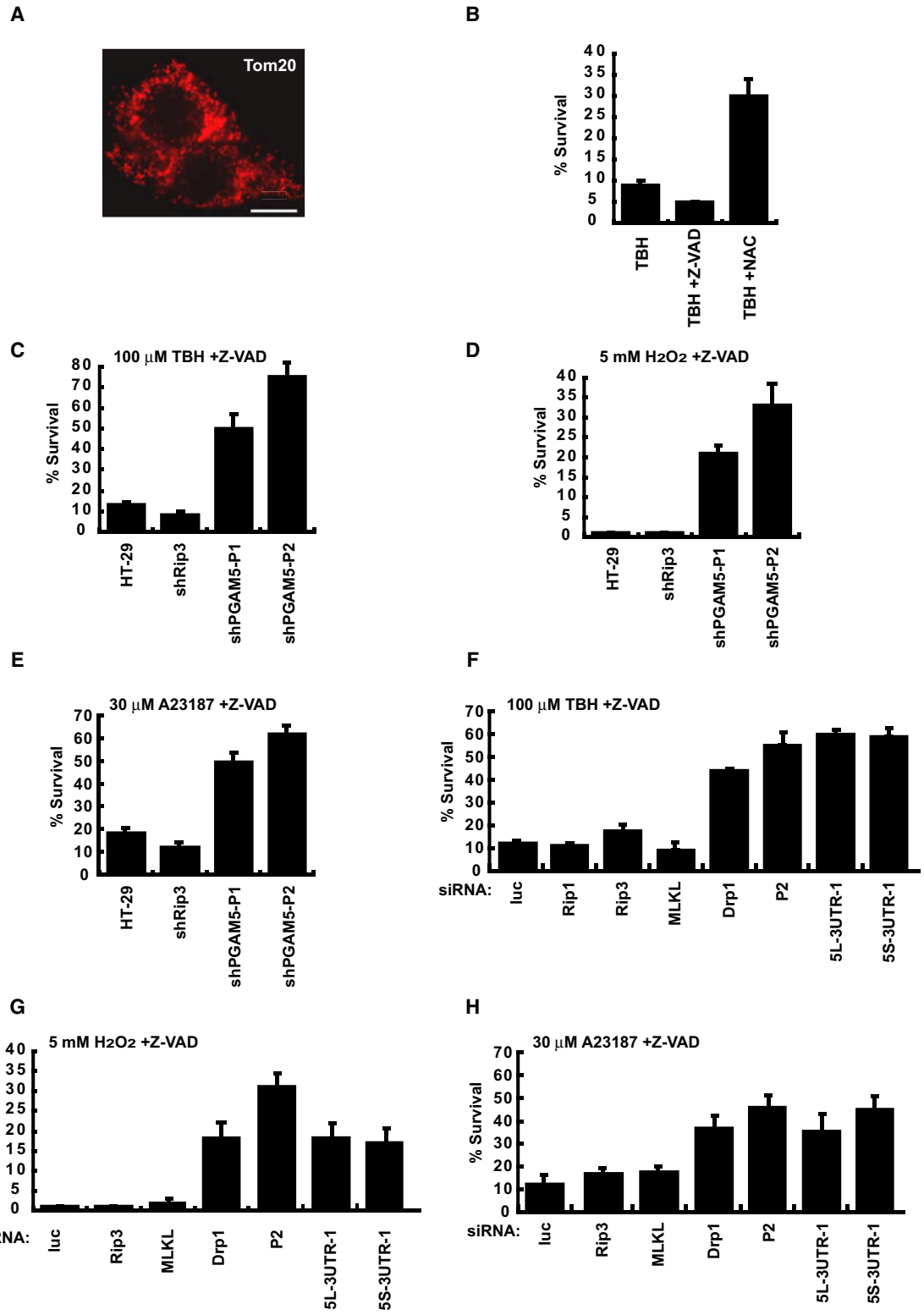

Figure 7. PGAM5 and Drp1 Are Required for ROS and Calcium Overload-Induced Necrosis

(A) HT-29 cells were treated with 100 μM of t-butyl-hydroperoxide (TBH) for 24 hr. Immunostaining was performed using an anti-Tom20 antibody.

(B) HT-29 cells were pretreated for 1 hr with Z-VAD or 5 mM N-acetyl-cysteine (NAC). The cells were then treated with 100 μM of TBH for 24 hr, and cell viability was determined.

Flag-HA Tandem Pull-Down and Mass Spectrometry

In total, 15 mg of P15 extract was incubated overnight with 300 μl of anti-Flag M2-agarose. After five washes with lysis buffer, the beads were eluted twice with 1 ml of lysis buffer containing 0.5 mg/ml 3xFlag peptide for 4 hr. The combined elution was incubated overnight with 50 μl anti-HA agarose. After five washes with lysis buffer, the beads were eluted with 200 μl of lysis buffer containing 0.5 mg/ml HA peptide for 4 hr. A total of 15 μl of 4 × SDS loading buffer was added to the final elution, and the mixture was boiled down to 60 μl and loaded into a 4%–12% gradient gel (Invitrogen, NP0321). All of the procedures were performed at 4°C unless otherwise stated. Silver staining was performed according to the manufacturer's instructions (SilverQuest silver staining kit, Invitrogen, LC6070).

Kinase Assay

Anti-Flag immunoprecipitation was performed as described above. After three washes with the kinase buffer (50 mM Tris [pH 7.5], 10 mM $MgCl_2$, 50 mM NaCl, 0.1% BSA, 100 μM ATP, and 1 mM DTT), the beads were incubated with 2 μCi of γ-^{32}P-ATP at 30°C for 1 hr with or without recombinant His-tagged PGAM5L. The reactions were then loaded onto a 12% SDS-PGAE gel and subject to autoradiography analysis. All of the buffers included a protease inhibitor cocktail from Roche, #11873580001, and phosphatase inhibitor mix (20 mM glycerol β-phosphate, 10 mM NaF, 0.5 mM sodium orthovanadate, and 5 mM sodium pyrophosphate).

Phosphatase Assay

Anti-Flag immunoprecipitation and kinase reactions with recombinant His-tagged PGAM5L were performed as described above without γ-^{32}P-ATP and the phosphatase inhibitor mix. The recombinant His-tagged PGAM5L was purified using Ni-NTA beads (QIAGEN). After three washes with phosphatase buffer (50 mM imidazole [pH 7.2], 0.2 mM EGTA, 0.02% 2-mecaptoethanol, and 0.1 mg/ml BSA), the Ni-NTA beads were incubated with 100 μM of a phospho-Thr peptide (RRApTVA, Promega) at 30°C for 1 hr. The released free phosphate was quantified using the Phosphatase Assay System from Promega (V2460).

GTPase Assay

A total of 1 mg of whole-cell extract was immunoprecipitated overnight with 20 μg of anti-Drp1 antibody (Santa Cruz, sc-32989) and 100 μl of protein A/G-agarose (Santa Cruz). After three washes with lysis buffer and three washes with GTPase buffer (50 mM Tris [pH 7.5], 2.5 mM $MgCl_2$, and 0.02% 2-mercaptoethanol), the beads were incubated with 0.5 mM GTP at 30°C for 1 hr. The released free phosphate was quantified using the PiColorLock Gold kit from Innova Biosciences.

For in vitro PGAM5L treatment, immunopurified Drp1 was incubated with 300 ng of recombinant PGAM5L in phosphatase buffer at 30°C for 1 hr. After three washes with GTPase buffer, the beads were incubated with 0.5 mM GTP at 30°C for 1 hr. The released free phosphate was quantified using the PiColorLock Gold kit.

SUPPLEMENTAL INFORMATION

Supplemental Information includes six figures and can be found with this article online at doi:10.1016/j.cell.2011.11.030.

ACKNOWLEDGMENTS

We would like to thank Drs. Steve McKnight, Joe Goldstein, and Mike Brown for support and encouragement; Dr. Ayako Suzuki for help with the 2D electrophoresis; Drs. Lai Wang, Agata Rybarska, and Gregory Kunkel for critical reading of the manuscript. This work was supported by the Howard Hughes Medical Institute and the National High Technology Projects 863 (2008AA022318) and 973 (2010CB835400) from Chinese Ministry of Science and Technology.

Received: June 23, 2011
Revised: October 25, 2011
Accepted: November 10, 2011
Published: January 19, 2012

REFERENCES

Breckenridge, D.G., Kang, B.H., Kokel, D., Mitani, S., Staehelin, L.A., and Xue, D. (2008). Caenorhabditis elegans drp-1 and fis-2 regulate distinct cell-death execution pathways downstream of ced-3 and independent of ced-9. Mol. Cell *31*, 586–597.

Cassidy-Stone, A., Chipuk, J.E., Ingerman, E., Song, C., Yoo, C., Kuwana, T., Kurth, M.J., Shaw, J.T., Hinshaw, J.E., Green, D.R., and Nunnari, J. (2008). Chemical inhibition of the mitochondrial division dynamin reveals its role in Bax/Bak-dependent mitochondrial outer membrane permeabilization. Dev. Cell *14*, 193–204.

Chang, C.R., and Blackstone, C. (2007). Cyclic AMP-dependent protein kinase phosphorylation of Drp1 regulates its GTPase activity and mitochondrial morphology. J. Biol. Chem. *282*, 21583–21587.

Cho, D.H., Nakamura, T., Fang, J., Cieplak, P., Godzik, A., Gu, Z., and Lipton, S.A. (2009a). S-nitrosylation of Drp1 mediates beta-amyloid-related mitochondrial fission and neuronal injury. Science *324*, 102–105.

Cho, Y.S., Challa, S., Moquin, D., Genga, R., Ray, T.D., Guildford, M., and Chan, F.K. (2009b). Phosphorylation-driven assembly of the RIP1-RIP3 complex regulates programmed necrosis and virus-induced inflammation. Cell *137*, 1112–1123.

Cribbs, J.T., and Strack, S. (2007). Reversible phosphorylation of Drp1 by cyclic AMP-dependent protein kinase and calcineurin regulates mitochondrial fission and cell death. EMBO Rep. *8*, 939–944.

Declercq, W., Vanden Berghe, T., and Vandenabeele, P. (2009). RIP kinases at the crossroads of cell death and survival. Cell *138*, 229–232.

Degterev, A., Hitomi, J., Germscheid, M., Ch'en, I.L., Korkina, O., Teng, X., Abbott, D., Cuny, G.D., Yuan, C., Wagner, G., et al. (2008). Identification of RIP1 kinase as a specific cellular target of necrostatins. Nat. Chem. Biol. *4*, 313–321.

Frank, S., Gaume, B., Bergmann-Leitner, E.S., Leitner, W.W., Robert, E.G., Catez, F., Smith, C.L., and Youle, R.J. (2001). The role of dynamin-related protein 1, a mediator of mitochondrial fission, in apoptosis. Dev. Cell *1*, 515–525.

He, S., Wang, L., Miao, L., Wang, T., Du, F., Zhao, L., and Wang, X. (2009). Receptor interacting protein kinase-3 determines cellular necrotic response to TNF-alpha. Cell *137*, 1100–1111.

Holler, N., Zaru, R., Micheau, O., Thome, M., Attinger, A., Valitutti, S., Bodmer, J.L., Schneider, P., Seed, B., and Tschopp, J. (2000). Fas triggers an

(C) Stable cell lines derived from HT-29 cells that express shRNA against RIP3 or PGAM5 were treated with 100 μM TBH and Z-VAD for 24 hr, and cell viability was determined.
(D) The cells as in (C) were treated with 5 mM H_2O_2 for 1 hr and replaced with fresh medium supplemented with Z-VAD. Cell viability was determined after 24 hr.
(E) The cells as in (C) were treated with 30 μM of calcium ionophore A23187 and Z-VAD for 24 hr, and cell viability was determined.
(F) HT-29 cells were transfected with three rounds of indicated siRNAs. Cell viability was determined after 24 hr treatment of 100 μM TBH and Z-VAD.
(G) The cells were prepared as in (F). Cell viability was determined as in (D).
(H) The cells were prepared as in (F). Cell viability was determined after 24 hr treatment of 30 μM A23187 and Z-VAD.
Data are represented as the mean ± STDEV of duplicates. Supported by Figure S5.

alternative, caspase-8-independent cell death pathway using the kinase RIP as effector molecule. Nat. Immunol. *1*, 489–495.

Imai, Y., Kanao, T., Sawada, T., Kobayashi, Y., Moriwaki, Y., Ishida, Y., Takeda, K., Ichijo, H., Lu, B., and Takahashi, R. (2010). The loss of PGAM5 suppresses the mitochondrial degeneration caused by inactivation of PINK1 in Drosophila. PLoS Genet. *6*, e1001229.

Jagasia, R., Grote, P., Westermann, B., and Conradt, B. (2005). DRP-1-mediated mitochondrial fragmentation during EGL-1-induced cell death in C. elegans. Nature *433*, 754–760.

Kaiser, W.J., Upton, J.W., Long, A.B., Livingston-Rosanoff, D., Daley-Bauer, L.P., Hakem, R., Caspary, T., and Mocarski, E.S. (2011). RIP3 mediates the embryonic lethality of caspase-8-deficient mice. Nature *471*, 368–372.

Lee, Y.J., Jeong, S.Y., Karbowski, M., Smith, C.L., and Youle, R.J. (2004). Roles of the mammalian mitochondrial fission and fusion mediators Fis1, Drp1, and Opa1 in apoptosis. Mol. Biol. Cell *15*, 5001–5011.

Lo, S.C., and Hannink, M. (2006). PGAM5, a Bcl-XL-interacting protein, is a novel substrate for the redox-regulated Keap1-dependent ubiquitin ligase complex. J. Biol. Chem. *281*, 37893–37903.

Lo, S.C., and Hannink, M. (2008). PGAM5 tethers a ternary complex containing Keap1 and Nrf2 to mitochondria. Exp. Cell Res. *314*, 1789–1803.

Micheau, O., and Tschopp, J. (2003). Induction of TNF receptor I-mediated apoptosis via two sequential signaling complexes. Cell *114*, 181–190.

Oberst, A., Dillon, C.P., Weinlich, R., McCormick, L.L., Fitzgerald, P., Pop, C., Hakem, R., Salvesen, G.S., and Green, D.R. (2011). Catalytic activity of the caspase-8-FLIP(L) complex inhibits RIPK3-dependent necrosis. Nature *471*, 363–367.

Olichon, A., Baricault, L., Gas, N., Guillou, E., Valette, A., Belenguer, P., and Lenaers, G. (2003). Loss of OPA1 perturbates the mitochondrial inner membrane structure and integrity, leading to cytochrome c release and apoptosis. J. Biol. Chem. *278*, 7743–7746.

Otera, H., and Mihara, K. (2011). Molecular mechanisms and physiologic functions of mitochondrial dynamics. J. Biochem. *149*, 241–251.

Smirnova, E., Griparic, L., Shurland, D.L., and van der Bliek, A.M. (2001). Dynamin-related protein Drp1 is required for mitochondrial division in mammalian cells. Mol. Biol. Cell *12*, 2245–2256.

Sugioka, R., Shimizu, S., and Tsujimoto, Y. (2004). Fzo1, a protein involved in mitochondrial fusion, inhibits apoptosis. J. Biol. Chem. *279*, 52726–52734.

Sun, L., Wang, H., Wang, Z., He, S., Chen, S., Liao, D., Wang, L., Yan, J., Liu, W., Lei, X., and Wang, X. (2011). Mixed lineage kinase domain-like protein mediates necrosis signaling downstream of RIP3 kinase. Cell *148*, this issue, 213–227.

Takeda, K., Komuro, Y., Hayakawa, T., Oguchi, H., Ishida, Y., Murakami, S., Noguchi, T., Kinoshita, H., Sekine, Y., Iemura, S., et al. (2009). Mitochondrial phosphoglycerate mutase 5 uses alternate catalytic activity as a protein serine/threonine phosphatase to activate ASK1. Proc. Natl. Acad. Sci. USA *106*, 12301–12305.

Temkin, V., Huang, Q., Liu, H., Osada, H., and Pope, R.M. (2006). Inhibition of ADP/ATP exchange in receptor-interacting protein-mediated necrosis. Mol. Cell. Biol. *26*, 2215–2225.

Trichonas, G., Murakami, Y., Thanos, A., Morizane, Y., Kayama, M., Debouck, C.M., Hisatomi, T., Miller, J.W., and Vavvas, D.G. (2010). Receptor interacting protein kinases mediate retinal detachment-induced photoreceptor necrosis and compensate for inhibition of apoptosis. Proc. Natl. Acad. Sci. USA *107*, 21695–21700.

Upton, J.W., Kaiser, W.J., and Mocarski, E.S. (2010). Virus inhibition of RIP3-dependent necrosis. Cell Host Microbe *7*, 302–313.

Vanlangenakker, N., Vanden Berghe, T., Krysko, D.V., Festjens, N., and Vandenabeele, P. (2008). Molecular mechanisms and pathophysiology of necrotic cell death. Curr. Mol. Med. *8*, 207–220.

Wang, L., Du, F., and Wang, X. (2008). TNF-alpha induces two distinct caspase-8 activation pathways. Cell *133*, 693–703.

Wang, C., and Youle, R.J. (2009). The role of mitochondria in apoptosis. Annu. Rev. Genet. *43*, 95–118.

Yoon, Y., Pitts, K.R., and McNiven, M.A. (2001). Mammalian dynamin-like protein DLP1 tubulates membranes. Mol. Biol. Cell *12*, 2894–2905.

Youle, R.J., and Strasser, A. (2008). The BCL-2 protein family: opposing activities that mediate cell death. Nat. Rev. Mol. Cell Biol. *9*, 47–59.

Zhong, Q., Gao, W., Du, F., and Wang, X. (2005). Mule/ARF-BP1, a BH3-only E3 ubiquitin ligase, catalyzes the polyubiquitination of Mcl-1 and regulates apoptosis. Cell *121*, 1085–1095.